- Article type: Paper
- Revised Date: October 2, 2017
- Words: 5,218
- Figures: 10
- Tables: 7

Use of a MEMS Accelerometer to Measure Orientation in a Geotechnical Centrifuge

Author 1

- Ryan D. Beemer, PhD
- ORCID: 0000-0002-9101-5325
- Centre for Offshore Foundation System, University of Western Australia, Crawley, Australia
- Work phone: +61 8 6488 2782
- Mobile phone: +61 0456 411 365
- Email: ryan.beemer@uwa.edu.au

Author 2

- Giovanna Biscontin, PhD
- ORCID: 0000-0002-4662-5650
- Department of Engineering, University of Cambridge, Cambridge, United Kingdom

Author 3

- Madhuri Murali, PhD
- ORCID: 0000-0002-1055-5072
- Project Engineer, Fugro Marine geo-Services, Inc., Houston, Texas

Author 4

- Charles P. Aubeny, PhD
- ORCID: 0000-0002-4032-6895
- Zachry Department of Civil Engineering, Texas A&M University, College Station, United States

Abstract (181 words)

Microelectromechanical systems (MEMS) accelerometers are becoming more prevalent in geotechnical engineering and geotechnical centrifuge modelling. In centrifuge experiments these sensors have shown great promise, but still exhibit limitations. This paper proposes a new methodology for the use of single-axis, low-g, high accuracy MEMS accelerometers to measure orientation of on object on the vertical rotational plane of centrifugal acceleration and Earth's gravity in a geotechnical centrifuge. The method specifically compensates for measured cross-axis acceleration by a MEMS accelerometer when in a high-g environment. This is done by determining the apparent internal misalignment of the MEMS sensing unit, relative to its packaging, from a high-g cross-axis calibration. The misalignment can then be used to correct the measured orientation of sensor relative to a centrifuge gravity vector. When compared to simplified approaches measurements of absolute orientation are improved by 0.98º and the standard deviation of measurements between multiple sensors is reduced by 0.73º. Overall, this new methodology significantly improves the accuracy of orientation measurements by a MEMS accelerometers in the geotechnical centrifuge, opening the door to use these inexpensive sensors in more experiments.

Keywords: Centrifuge modelling, Laboratory equipment, Monitoring

List of Notation

Y	centrifuge axial coordinate
r	centrifuge radial coordinate perpendicular to the centrifuge axis, Y
ω	angular velocity of the centrifuge
x	local horizontal coordinate of model
y	local width coordinate of model
z	local vertical coordinate of model
x_{sensor}	sensor x-coordinate

y_{sensor} sensor x-coordinate

z_{sensor} sensor z-coordinate

x_M Apparent x-coordinate of sensor due to misalignment

R vertical rotational inertial 2D reference frame defined by the centrifuge axis, Y, and centrifuge radial axis, r

g magnitude of centrifuge gravity vector, $\tilde{g}$, in the vertical rotational plane

g_c magnitude of centrifugal acceleration vector, $\tilde{g}_c$

g_e magnitude of Earth's gravity vector, $\tilde{g}_e$

α angle between a centrifuge gravity vector, $\tilde{g}$, and the centrifuge radial coordinate, r

β angle between a centrifuge gravity vector, $\tilde{g}$, and the local vertical coordinate, z

ξ angle between the local vertical coordinate axis, z, and the centrifuge radial coordinate, r

V_n measured voltage by a MEMS accelerometer due to an acceleration applied in its measurement direction

V_0 measured zero-g voltage by a MEMS accelerometer when no acceleration is applied

V_α measured zero-g voltage by a MEMS accelerometer with apparent internal misalignment and a cross-axis acceleration of 1 g is applied

V_x is the measured voltage from an applied cross-axis acceleration, a_x

C_F calibration factor relating applied acceleration to measured voltage (V/g)

$C_{F\alpha}$ calibration factor relating applied acceleration to measured voltage (V/g) with internal misalignment and a zero-g voltage of V_α

C_x cross-axis acceleration correlation factor

θ_n angle of MEMS accelerometer z-coordinate, z_{sensor}, to the centrifuge acceleration vector $\tilde{g}$

θ_t angle of MEMS accelerometer z-coordinate, z_{sensor}, to the model z-coordinate, z

θ_α the apparent internal angular misalignment of the MEMS accelerometer in the x-z plane

a_n an acceleration applied in-line with the sensors measurement directions

a_{meas} acceleration measured by the MEMS accelerometer

a_{cross} component of acceleration perpendicular to the MEMS accelerometer measurement direction, z_{sensor}, measure by the sensor

a_{temp} acceleration measured by the MEMS accelerometer due to temperature change of the sensor

a_x magnitude of an applied cross-axis acceleration in z_{sensor}

Vertical rotational plane A vertical plane defined by centrifuge axis, Y, and centrifuge radial coordinate, *r*

1. Introduction

Microelectromechanical systems (MEMS) accelerometers have become a ubiquitous part of everyday life, being found in mobile phones, tablets and cars. Their prevalence in part is due to the mass production silicon fabrication techniques used to manufacture them (Spangler and Kemp 1996), which allows for low relative costs. Aside from their cost, MEMS accelerometers are an attractive option for geotechnical engineers because to their ability to measure persistent acceleration. Unlike piezoelectric accelerometers, MEMS can measure a vector of constant acceleration and their orientation relative to this vector.

The adaptation of MEMS into civil engineering has been advocated since at least 2000 (Oppenheim et al. 2000). In geotechnical engineering, specifically, MEMS accelerometers have served two main purposes: dynamic measurements of sensor motion and quasi-static measurements of sensor orientation relative to gravity. MEMS accelerometers have been used both in the field and the laboratory by geotechnical engineers. Examples include: measuring wave propagation with custom packaged MEMS accelerometer circuits (Hoffman et al. 2006; Bhattacharya et al. 2012), measuring soil mass deformation using the shape-acceleration array (Bennett et al. 2009), measuring acceleration in liquefaction field tests (Saftner et al. 2008), measuring penetrometers deceleration for characterizing offshore sediments (Stark et al. 2009), and monitoring the installation of dynamically embedded plate anchors (Blake and O'Loughlin 2015).

An area of geotechnical testing which has recently seen growth in the use of MEMS accelerometers is centrifuge scale modelling. Results from this paper were used by Beemer (2016) to measure caisson cycling at rotational amplitudes of less than 0.5 degrees, Fig. 1. Other examples include: evaluation of MEMS accelerometers in dynamic centrifuge testing (Stringer et al. 2010), seismic evaluation of pile reinforced slopes (Al-Defae and Knappett 2014), measuring model radial distance from the centrifuge axis and dead reckoning of a dynamically penetrated anchor in-line with centrifuge gravity (O'Loughlin et al. 2014), measurements of monopile rotation using high-g accelerometers (Lau 2015), and large angle anchor orientation in sand (Chow et al. 2015).

Though these initial cases have been quite successful, there is still room for improvement. Stringer et al. (2010) noted that spurious accelerations were measured during centrifuge spin up and residual velocities, after integration of acceleration, were also measured at completion of the experiment, when the sensors were still. The accuracy of orientation measurements with MEMS accelerometers has also been relatively low. Chow et al. (2015) reported orientation with errors of ±1º-2.5º. While Lau (2015) found it necessary to amplify the output of a 35 g MEMS accelerometer by a gain of 10 to collect useable data, and even with this additional circuity there were cases where their accuracy was too low to be of use. If the angular accuracy of the MEMS accelerometers in high-g could be improved when used in the centrifuge a number of interesting and difficult problems could be investigated, such as: measuring rotation of monopile for offshore wind turbines where serviceability tilts are limited to 0.5º (DNV 2007) and lateral spreading of shallow slopes. In the past, slopes with angles as low as 0.6º (Taboada-Urtuzuástegui and Dobry 1998) and 3º (Stringer et al. 2010) have been studied in the centrifuge.

To date, measurements of orientation in the centrifuge (Lau 2015; Chow et al. 2015; Allmond et al. 2014) have utilized a simple sinusoidal relationship to relate measured acceleration to orientation relative to centrifuge gravity. This process was outlined by Allmond et al. (2014) who showed the method resulted in good correlation to angular measurements from linear displacement transducers, but little discussion of initial or absolute orientation of the sensor to centrifuge gravity is provided. Their method also specifically excludes measured cross-axis acceleration, which was later suggested to be significant at accelerations as low as 10 g (Beemer et al. 2015). Additionally, measured cross-axis accelerations could explain the extraneous accelerations measured during spin up by Stringer et al. (2010). This paper expands on earlier quasi-static orientation theories by compensating for measured cross-axis accelerations created by the apparent internal misalignment of the MEMS sensing unit within the housing.

It is also worth noting that measured cross-axis accelerations are incorporated into accelerographs measurements of earthquake motions (Wong and Trifunac 1977). Traditionally, accelerographs rely

on three single degree of freedom pendulums to measure acceleration. In this simple macro-mechanical design cross-axis effects can be broken into two components: cross-axis sensitivity and internal misalignment. Cross-axis sensitivity is attributed to acceleration applied cross-axis to the pendulum's designated degree of freedom when it under goes a pseudo-static rotation see (Wong and Trifunac 1977). Internal misalignment of the pendulum's measurement axis with respect to the accelerograph's local coordinates will also result in a measured cross-axis acceleration. Complete solutions based on pendulum physics and coordinate rotation relative to Earth's gravity are available to calibrate for both cross-axis effects and internal misalignment; however, these are not readily applicable to MEMS accelerometers.

The main reason accelerograph methods are not applicable to MEMS accelerometers is that they do not rely on pendulums to measure acceleration. Their micromechanical structures are actually quite varied and their exact design is not typically provided to the user. Many systems are based on spring mass systems, with varying means of converting proof mass deflection to an electrical signal (Shaeffer 2013). There are even designs where a proof mass is not even needed; heat convection MEMS accelerometers rely on temperature gradients within a heated micro-chambers to measure acceleration (Leung et al. 1997; MEMSIC 2007). A second reason accelerograph methods are not applicable, is that MEMS accelerometers zero-g voltage cannot be separated from a voltage measured when a cross-axis acceleration of 1 g is applied, under typical laboratory conditions. The method presented in this paper overcomes these issues by assuming any cross-axis sensitivity of the MEMS is due solely to an apparent internal misalignment and through the performance of a high-g cross-axis calibration.

This paper examines the use of MEMS accelerometers to measure orientation within a geotechnical centrifuge and presents a methodology for measuring sensor orientation relative to centrifuge gravity to a high accuracy. This investigation is supported by results from high-g cross-axis experiments on single-axis low-g accelerometers. It was found that measured cross-axis acceleration due to apparent internal misalignment of the sensor has a significant impact on

measurements of absolute angular orientation relative to centrifuge gravity.

2. Background

2.1 The Centrifuge Gravity Field

In this paper centrifuge gravity is treated as 2-dimensional on the vertical rotational inertial reference frame of the centrifuge axis and the radial coordinate and is the resultant of centrifugal acceleration, g_c, and Earth's gravity, g_e, Equations 1 – 2. Any out-of-plane accelerations are considered beyond the scope of this paper.

$$g_c = \omega^2 r \quad (1)$$

$$g = g_c \cdot \hat{\imath} + g_e \cdot \hat{\jmath} \quad (2)$$

where: g_c is centrifugal acceleration, ω is rotational velocity, r is radial coordinate from the centrifuge axis, g is centrifuge gravity, and g_e is Earth's gravity

Additionally, this paper incorporates gravity field rotation due to tilt of a free-swinging centrifuge basket as presented in Beemer et al. (2016). That is, rotation of the basket due to applied moments about the basket hinge, such as from cabling and hydraulic hosing or changes to its centre-of-gravity, will result in rotation of the model's coordinates, ξ, relative the radial coordinate, r. This will result in any centrifuge gravity vector, $\tilde{g}$, being at an angle β to the model local coordinates (x,z) as shown in Fig. 2. In the figure, α is the angle of centrifuge gravity to the centrifuge radial

coordinate, *r*, and *R* is the rotational reference frame.

2.2 MEMS Accelerometers

MEMS accelerometers convert a measured acceleration to electrical output. Unlike piezo-electric sensors, an input voltage must be applied for the sensor to work. Under a single-ended configuration they will output a constant signal at zero-g, known as the zero-g voltage, V_0. An acceleration measurement is then taken as:

$$a_n = (V_n - V_0) \cdot C_F \quad (3)$$

where: a_n is an acceleration applied in-line with the sensor's measurement directions, V_n is the voltage measured due to an acceleration in-line with the sensor and C_F is the calibration factor due to an acceleration applied in-line with the sensor.

The calibration factor is the linear relationship between measured voltage and applied acceleration and can be determined in two ways. The first is to apply quantities of known acceleration directly in-line with sensor's measurement direction and record the output voltage, Eq. 4. This could be done by placing the sensor at a known radius in a geotechnical centrifuge spinning at a precise angular velocity. This method allows for a MEMS accelerometer to be calibrated over its entire sensing range and ensures no cross-axis acceleration is measured. When calibrating low-g accelerometers with centrifugal acceleration, the angle of the vector relative to the sensor must be considered. In a drum centrifuge (or beam centrifuge with a fixed basket) the angle of centrifuge gravity, α, to the accelerometer's measurement direction will be 45° at 1 g, 11.3° at 5 g and 5.7° at 10 g. Care must also be taken in beam centrifuges with free-swinging baskets. A basket is

susceptible to tilting at low magnitudes of centrifugal acceleration (Beemer et al. 2017) and any angle, β, between the sensor and centrifuge gravity will need to be corrected for.

$$C_F = \frac{\Delta a_n}{\Delta V_n} \quad (4)$$

where: C_F is the calibration factor

The second and more frequently used method is to rotate the accelerometer in Earth's gravity such that the applied acceleration ranges between -1 g and 1 g. A multi-point calibration can be done by the fabrication of an angular calibrator such as the 3D printed one shown in Fig. 3, used in the laboratories at the University of Western Australia and Texas A&M University. It allows for a seven calibration points from 0° to 90°, at 15° increments. The disadvantage of this approach is that the magnitude of acceleration applied to a sensor is limited to ±1 g, which is just a fraction of the range of a 5 g or 10 g MEMS accelerometer. This method is typically preferred because it is cheaper and more time effective to calibrate the accelerometers outside the centrifuge, especially given it is best practice to re-calibrate sensors on a regular basis.

3. Accelerometer Orientation Theory in the Centrifuge

A quasi-static assumption is used in this derivation. As such, kinematic accelerations from relative displacement or rotation of the accelerometer are not considered and are outside the scope of this paper. This includes Coriolis acceleration, which is dependent on sensor velocity along the centrifuge radial coordinate, *r*. For more on Coriolis accelerations in the centrifuge see Madabhushi

(2015), Randolph et al. (1991), and Schofield (1980).

3.1 Sensor Measurements and Geometry

Measurements of orientation by a single-axis MEMS accelerometer are made relative to an acceleration vector, in this case centrifuge gravity. Ideally, when the sensor is perpendicular to a centrifuge gravity vector it should read zero and when it is in-line with a centrifuge gravity vector it should read its magnitude. However, in a high-g environment this is not the case. Actual measurements from a MEMS accelerometer are affected by a number of factors, as shown in Fig. 4: applied centrifuge gravity, $\tilde{g}$, measured acceleration due to sensor change in temperature, a_{temp}, and any measured accelerations due to cross-axis sensitivity, a_{cross}. The measured cross-axis acceleration results from the sensor's tendency to measure a portion of an acceleration applied perpendicular to its measurement direction, z_{sensor} in Fig. 4. Combining these, the measured acceleration from a single-axis MEMS accelerometer will be:

$$a_{meas} = a_n + a_{cross} + a_{temp} \quad (5)$$

where: a_{meas} is the acceleration measured by the MEMS accelerometer, a_{cross} is the measured cross axis acceleration and a_{temp} is the acceleration measured due to temperature change of the sensor

If it is then assumed that all measured cross-axis acceleration can be modelled as an internal misalignment of the MEMS sensing unit within the package, Fig. 5, Equation 5 can be presented dependent on the sensor's angle to centrifuge gravity, Equation 6. This assumption appears valid given the linearity of measured cross-axis acceleration with applied centrifuge gravity presented by Beemer et al. (2015).

$$a_{meas} = g \cdot \sin(\theta_n + \theta_\alpha) + a_{temp} \quad (6)$$

where: θ_α is the apparent misalignment and θ_n is the angular orientation of the sensor relative to centrifuge gravity

This is similar to the solution provided by Allmond et al. (2014); however, temperature effects and measured cross-axis acceleration due to sensor internal misalignment are included. To determine a MEMS accelerometer's orientation relative to a centrifuge gravity vector, $\tilde{g}$, Equation 6 can be solved for θ_n:

$$\theta_n = \arcsin\left(\frac{a_{meas} - a_{temp}}{g}\right) - \theta_\alpha \quad (7)$$

The measured acceleration due to variation in sensor temperature is often insignificant (see Discussion); however, for completeness it is included in the final solution, Equation 7.

3.2 Cross-Axis Sensitivity due to Internal Misalignment

To determine the absolute orientation of an MEMS accelerometer in a high-g environment it is necessary to assess the effects of cross-axis sensitivity. It is assumed that all of the measured cross-axis acceleration is due to the apparent internal misalignment of the sensing unit within the package in the x-z plane, about the y_{sensor} axis, Fig. 5. In actuality, cross-axis sensitivity can be the result of both intrinsic mechanical effects and internal misalignment. If the entirety of the reported cross-axis sensitivity for the 10 g accelerometers used in this paper, Table 1, is assumed to be the result of

misalignment then an apparent internal misalignment of ±2.86° is possible.

The component of cross-axis acceleration in the sensor's measurement direction for of an applied cross-axis acceleration, a_x, in the z_{sensor} direction, Fig. 5, will be:

$$a_{cross} = \sin(\theta_\alpha) \cdot a_x \quad (8)$$

where: a_x is the magnitude of an applied cross-axis acceleration

Given an apparent internal misalignment, the expected measured misalignment of the sensor from Equation 3 is:

$$a_{cross} = (V_x - V_0) \cdot C_F \quad (9)$$

where: V_x is the measured voltage from an applied cross-axis acceleration, a_x

Setting Equation 8 equal to Equation 9 we can solve for the misalignment:

$$\theta_\alpha = \arcsin\left(\frac{V_x - V_0}{a_x} \cdot C_F\right) \quad (10)$$

It can be seen that the first factor in the trigonometric function is the gradient of the measured cross-

axis voltage to applied cross-axis acceleration. For the purpose of sensor calibration it is more convenient and beneficial to define Equation 10 in terms of this quantity:

$$\theta_\alpha = \arcsin(C_x \cdot C_F) \quad (11)$$

$$C_x = \frac{\Delta V_x}{\Delta a_x} \quad (12)$$

where: C_x is the cross-axis calibration factor

3.2 Internal Misalignment and the MEMS 1-g Calibration Method

Calibrating a MEMS accelerometer by rotating it in Earth's gravity, Fig. 3, will incorporate the apparent internal misalignment into the calibration variables. Therefore, it is necessary to assess the effect misalignment on the zero-g voltage, V_0, and calibration factor, C_F, and how it can be calculated when the 1-g calibration method is used.

It is assumed that the zero-g voltage is assessed by holding the sensor's measurement axes perpendicular to Earth's gravity. Given this, the zero-g voltage including misalignment is:

$$V_\alpha = V_0 + \frac{\sin(\theta_\alpha) \cdot 1\ \mathrm{g}}{C_F} \quad (13)$$

With a small angle assumption:

$$V_\alpha = V_0 - \frac{\theta_\alpha}{C_F} \quad (14)$$

where: V_α is the zero-g voltage with apparent internal misalignment and 1-g of applied cross-axis acceleration

Depending on the sensitivity and noise of the individual sensor, it may be appropriate to assume the second term in Equation 14 is negligible; however, this should be assessed on a case by case basis. Next, it is necessary to assess the effect of misalignment on the calibration factor C_F, Equation 4. If the sensor is internally misaligned as in Fig. 5, the measured calibration factor with a misalignment θ_α will be:

$$C_{F\alpha} = \frac{1\ g \cdot \sin(\theta_2 + \theta_\alpha) - 1\ g \cdot \sin(\theta_1 + \theta_\alpha)}{V_2 - V_1} \quad (15)$$

where: $C_{F\alpha}$ is the calibration factor with internal misalignment and a zero-g voltage of V_α, θ_i are the angles at which the accelerometers are calibrated, and V_i are sensor output voltages at angles θ_i

Substituting in trigonometric identities and simplifying:

$$C_{F\alpha} = \frac{(\sin(\theta_2)\cos(\theta_\alpha) + \cos(\theta_2)\sin(\theta_\alpha)) - (\sin(\theta_1)\cos(\theta_\alpha) - \cos(\theta_1)\sin(\theta_\alpha))}{V_2 - V_1}$$

16.

A small angle assumption can then be applied, assuming as well that $\cos(\theta_\alpha < 3°) = 1$:

$$C_{F\alpha} = \frac{\sin(\theta_2) - \sin(\theta_1) + \cos(\theta_2)\,\theta_\alpha - \cos(\theta_1)\,\theta_\alpha}{V_2 - V_1}$$

17.

Rearranging Equation 17 produces the following:

$$C_{F\alpha}\left(\frac{V_2 - V_1}{\sin(\theta_2) - \sin(\theta_1)}\right) = 1 + \theta_\alpha\left(\frac{\cos\theta_2 - \cos\theta_1}{\sin\theta_2 - \sin\theta_2}\right)$$

18.

Upon inspection it can be seen that the second factor on the left-hand side is inverse of the calibration factor, Equation 4. Additionally, θ_1 and θ_2 can be set to 0° and 90°, respectively, encompassing the full 1-g calibration range. Substituting and simplifying:

$$C_{F\alpha} = C_F(1 - \theta_\alpha)$$

19.

This shows that the internal misalignment has an impact on the calibration factor. For an apparent misalignment of 2° the error could be up to 3.5%.

With $C_{F\alpha}$ now known the misalignment, Equation 11, can be updated with Equation 19:

$$\theta_\alpha = \arcsin\left(C_x \cdot \frac{C_{F\alpha}}{1-\theta_\alpha}\right) \quad (20)$$

Applying a small angle assumption and rearranging:

$$\theta_\alpha - {\theta_\alpha}^2 = C_x \cdot C_{F\alpha} \quad (21)$$

Knowing that the misalignment, θ_α, will be less than 0.5 radians, Equation 21 can be solved with the quadratic formula:

$$\theta_\alpha = \frac{1-\sqrt{1-4\cdot C_x \cdot C_{F\alpha}}}{2} \quad (22)$$

To obtain the sensor misalignment, θ_α, the corrected calibration factor, C_F, and the zero-g voltage, V_0, all that is require is for a user to measure the cross-axis correlation factor, C_x, by measuring the output voltage over a range of applied cross-axis accelerations.

It is also possible for the MEMS unit within the sensor package to be misaligned in the x-y plane,

about the z_{sensor} axis, and in the y-z plane, about the about the x_{sensor} axis. It can be shown the impact of these internal misalignments are insignificant, for small angles, but these solutions are considered outside the scope of this paper.

3.4 Orientation Relative to Basket Local Coordinates

As noted previously the MEMS accelerometer orientation, θ_n, is relative to the centrifuge gravity vector at the location of the sensor. To determine the orientation relative to the local vertical coordinate, *z*, it is necessary to take into account rotation, β, of the model local coordinate (*x*,*z*) relative to a gravity vector, $\tilde{g}$. This rotation could be due to an applied moment about the basket hinge and/or movement of the basket's centre of gravity. The orientation of the sensor with respect to the local coordinate system (*x*,*z*) as in Fig. 4 can then be defined as:

$$\theta_t = \theta_n - \beta \quad (23)$$

Substituting into Equation 7:

$$\theta_t = \arcsin\left(\frac{a_{meas} - a_{temp}}{g}\right) - \theta_\alpha - \beta \quad (24)$$

where: θ_t is the orientation of the sensor relative to the local (x,z) coordinate and β is the angle between the centrifuge gravity vector, $\tilde{g}$, and the local vertical coordinate, *z*

4. Validation Testing Program

The MEMS accelerometer selected to be the representative model is the MEMSIC CXL10GP1 single-axis accelerometer (MEMSIC n.d.) with a ± 10 g range, to further be referred to as 10 g Accelerometer; nine were used in the experiment. A single axis Silicon Design Model 2012 (Silicon Design Inc. 2013) with ± 100 g range of was used to measure applied acceleration, to be referred to subsequently as 100 g Accelerometer. Technical specifications for the 10 g and 100 g accelerometers can be found in Table 1.

Experiments were conducted in the 150 g-ton, 2.7 m nominal radius, beam type centrifuge at Rensselaer Polytechnic Institute in Troy, NY (Elgamal et al. 1991). Three custom 3D printed ABS plastic Test Platforms were used to carry the nine 10 g Accelerometers while the 100 g accelerometer was mounted to a separate platform, Fig. 6. The initial calibration factors and zero-g voltage with apparent internal misalignment are provided in Table 2. The 10 g Accelerometer platforms each carried three 10 g Accelerometers: two parallel to the basket floor and one inclined at 4º. All of the platforms were secured to the floor of the metal centrifuge basket with small (adhesive backed) rare earth magnets. The platforms were centred in the basket such that their x-z plane aligned with the plane of the centrifugal acceleration and Earth's gravity (*r*,Y), Fig. 7.

Three experiments were conducted. Each involved a single spin of the centrifuge where gravity, $\tilde{g}$, was stepped up in order to record the magnitude of acceleration measured by the 10 g Accelerometers. Accelerations were selected at regular intervals decreasing in step size at higher-g levels. Applied accelerations were monitored with the 100 g Accelerometer, Table 3. It was assumed that angle β between the centrifuge gravity, $\tilde{g}$, at the sensors and the model local coordinates was sufficiently small as not to impact measurements. Applied accelerations were not incremented at whole numbers because the sensors were beyond the centrifuge nominal radius which the control software uses when setting the rotational velocity. Between the experiments the 10 g Accelerometers were rotated from the zero degree spots on the platform to the four degree spots as outlined in Table 4, platforms are as numbered in Fig. 6.

5. Results

A cursory examination of the data collected from the sensors held at zero degrees in Experiment Three provided some interesting results, Fig. 8. If the assumption that measured cross-axis acceleration were insignificant were true all of the sensors would have recorded zero voltage over the course of the experiment. However, it can be clearly seen this was not the case. Cross-axis acceleration up to 475 mV was measured, in the case of M7, which is 12% of the 10 g Accelerometer output voltage range, Table 1. It can also be seen that magnitude of measured cross-axis acceleration is not the same for all sensors and can even be negative, as in the case of M8. This variation indicates that the measurements were not simply due to tilt of the centrifuge basket, ξ.

5.1 Cross-Axis Correlation and Senor Internal Misalignment

Initial calibration of internal misalignment showed consistent differences in measurements in Experiment One relative to Experiments Two and Three, Table 5. This uniformity indicates that the angle of centrifuge gravity relative to the sensors vertical axis, β, was 0.22° larger during Experiment One. This was due to the centrifuge basket being tilted at a different angle during that specific test. Any variation in β will have the same result as an apparent internal misalignment, θ_α, and can be corrected for. It was assumed that the angle β during Experiment Two and Three was closer to zero and Experiment One was correct for a 0.22° angle.

A nearly linear relationship can be seen between measured cross-axis acceleration, a_{cross}, and centrifuge gravity, $\tilde{g}$, Fig. 9, especially at higher accelerations. Linear curve regression fitting was carried out for data above 65g for all experiments, to determine the cross-axis calibration factors, Table 6. These specific sensors were being calibrated for use in a 70 g experiment. It can be seen that the correlations show a high order of linearity, with M8 being the lowest with an R^2 of 0.973.

Measured misalignments, corrected calibration factors C_F and corrected zero-g voltages are

provided in Table 6. The apparent misalignment lies within manufacture specification, Table 1, ranging from -0.16° to 1.61° with a mean and standard deviations of 0.86° and 0.62°, respectively.

5.2 Model Validation

As previously noted, three of the nine 10g Accelerometers were held at a four degree angle during each experiment to test the hypothesis that measured cross-axis acceleration could be corrected for apparent misalignment. Fig. 10 presents the results, which are grouped by testing platform and tabulated in Table 7. Temperature effects were considered negligible and a temperature correction was not included (see discussion for more).

The results of the comparison clearly show that the cross-axis sensitivity is not negligible and contributes significantly to the magnitude of the measured angle. The average measurement of the 4º shelves is 3.02º when cross-axis sensitivity is neglected and 3.94º when it is considered. This is a 23% improvement in measurement precision, if the 3D printed platforms are indeed at an angle of 4º (see Discussion). More significant, however, is the scatter in the uncorrected results when comparing sensors, as seen in Fig. 10. For measurements where cross-axis effects are ignored, the standard deviation in the measurement of the platform angle is 0.73º, on average, while it is only 0.02º when a correction is made for misalignment. Though in absolute terms this error is not large, it is significant relative to the desired measurement quantity in serviceability limits.

6. Discussion

6.1 Sensor Accuracy

Accuracy of orientation measurements with MEMS accelerometers is dependent on the data acquisition system (DAQ), sensor accuracy, sensor orientation, and magnitude of centrifuge gravity, $\tilde{g}$. In general, any sensor will only be as accurate as the measurement capabilities of the DAQ

sampling it; this has been specifically discussed for MEMS accelerometers by O'Loughlin et al. (2014). Each model of MEMS accelerometer will have an intrinsic measurement accuracy dependent on its output noise and offset. Sensor angular accuracy will be highly impacted by the initial orientation of the accelerometer. If the sensors measurement direction is initially in-line with centrifuge gravity a low accuracy, high range sensor will be required. However, if the sensor is initially aligned perpendicular to gravity a high accuracy, low range accelerometer can be used. Additionally, the sinusoidal functions relating centrifuge gravity to orientation are more variable when rotating into an acceleration vector than away from it. That is, the sine of a small angle is more variable than the cosine of a small angles. The accuracy of orientation measurements is also highly dependent on the magnitude of centrifuge gravity, as seen in Equation 24. Measurements of tilt from a MEMS accelerometer will increase in accuracy for increasing magnitudes of centrifuge gravity; this in turn will decrease the accelerometer's angular range. For example, if the 10 g Accelerometer accuracy is taken as three time the noise, Table 1, then its accuracy would be approximately 0.12º at 50 g and 0.06º at 100 g while its range would be approximately 11.54º at 50 g and 5.74º at 75 g.

6.2 Influence of Temperature on Sensor

As seen in Table 1, environmental temperature can influence the reading of MEMS accelerometers. Though this effect should be considered on a case by case basis, in general it should be minimal. This is in part due to the fact that major beam centrifuges are ventilated to prevent excessive temperatures (Elgamal et al. 1991; Ellis et al. 2006; Madabhushi 2015; Randolph et al. 1991; Schofield 1969; Black et al. 2014). From the literature, a worst case temperature variation for a centrifuge experiment appears to be taking a sensor from room temperature (25º C) to a refrigerated centrifuge model. Barrette et al. (1999) reduced a centrifuge model's temperature to -10º C, or a differential of 35º C, from room temperature. Given the 10g Accelerometer, Table 1, this would result in an approximate apparent measured angle of about 0.34º at 50 g. In this case it could be

reasonable to include the effect of temperature.

6.3 Experimental Validation of Model

Results from the validation show that the proposed model can be used to measure orientation in the centrifuge environment and that the inclusion of cross-axis sensitivity significantly improves measurements of orientation. Measured angle with the cross-axis correction of all the platforms were close to the design angle of 4º: Platform One was 3.81º, Platform Two was 4.03º, and Platform Three was 3.96º, or a 0.09º on average difference with most of the error in Platform One. This is a significant improvement over the 0.98º on average difference when cross-axis effects from apparent misalignment are ignored. Even more significant is that the average standard deviation of the measurement of these 4º platforms across all spins/experiments is 0.02º, on average, with the cross-axis correction and is found to be 0.73º, without cross-axis correction.

Given the low standard deviation in the platform measurements across all the experiments it appears the 0.19 error in Platform One is due to the tolerances in the 3D printing process. The tolerance in 3D printing processes of the platforms was ±0.127 mm (Stratasya 2015). Given this, the maximum possible error between the two legs, 70 mm apart, holding the sensor at 4º would be 0.254 mm and the maximum angular error would be 0.21º and this could account for all the error seen on Platform One tests. Additional error could be introduced from the deformation of the platform under high-g or by tolerance in the thickness of the rare earth magnets used to fix the platforms to the centrifuge basket. It is recommended that calibration platforms are constructed to a higher precision when working with these high accuracy sensors.

8. Conclusions

A number of conclusions can be drawn from the updated quasi-static orientation theory for single-axis MEMS accelerometers, the determination of cross-axis correlation factors, and the validation

experiment.

1. Single-axis MEMS accelerometers will measure significant magnitudes of cross-axis acceleration as a reaction to centrifuge gravity applied perpendicular to their measurement direction, Fig. 10. This can be attributed to an apparent misalignment of the sensing unit within the sensor package, Table 6. In these experiments a maximum error of 1.69º (0.98º on average) was seen when cross-axis acceleration from apparent internal misalignment was neglected, Table 7. Additionally, a standard deviation of 0.73° was seen in measurements when cross-axis acceleration was neglected, instead of the 0.02° when included. Errors of this magnitude would be significant for experiments where serviceability limits are of concern or experiments on shallow slopes.

2. The apparent internal misalignment of a MEMS accelerometer can be measured with a high-g cross-axis correlation, Equation 11-12 when the sensor is calibrated directly in-line with its measurement direction (this could be done in a centrifuge) and Equations 12 and 22 when the accelerometer is calibrated by rotating in Earth's gravity, Fig. 3. The measured misalignment can then be used to correct the reading of absolute orientation from a MEMS accelerometer used in the high-g environment of a geotechnical centrifuge, Equation 24.

3. Low-g single-axis MEMS accelerometers can be used to make fine measurements of orientation in a high-g environment when rotated into centrifuge gravity. In this paper it was possible to measure the absolute orientation of a platform constructed at a 4° angle to the basket floor to a standard deviation/accuracy of 0.02° while centrifuge gravity was greater than 65 g, Table 7. In fact it appears that they were sensitive enough to measure the tolerances in the 3D printing process used to create the calibration platforms.

Acknowledgements

The authors would like to acknowledge support from the National Science Foundation for the

project *Capacity and Performance of Foundations for Offshore Wind Towers*, Award Number: 1041604. The authors would like to thank the Department of Aerospace Engineering at Texas A&M University for use of their 3D printer and the faculty and staff in the Department of Civil and Environmental Engineering at Rensselaer Polytechnic Institute for their assistance.

References

Al-Defae, A. & Knappett, J., 2014. Centrifuge modeling of the seismic performance of pile-reinforced slopes. J. Geotech. and Geoenviron. Eng. ASCE **140**(**6**): 1–13

Allmond, J.D., Hakhamaneshi, M., Wilson, D.W. & Kutter, B.L., 2014. Advances in measuring rotation with MEMS accelerometers. *Proc. of the 8th Int. Conf. on Phys. Model. in Geotech.* (C. Gaudin & D. White (eds.)). CRC Press, Perth, pp. 353–359.

Barrette, P.D., Phillips, R., Clark, J.I., Crocker, G. & Jones, S.J., 1999. Flexural behavior of model sea ice in a centrifuge. J. of Cold Reg. Eng. ASCE **13**(**3**): 122–138

Beemer, R.D., 2016. *Experimental studies of squat gravity caissons and piles for offshore applications*. Texas A&M University.

Beemer, R.D., Aubeny, C.P. & Biscontin, G., 2017. Centrifuge 2D gravity on a vertical rotational reference frame. Int. J. Of Phys. Modell. in Geotech. (Forthcoming).

Beemer, R.D., Murali, M., Biscontin, G. & Aubeny, C.P., 2015. Theory on measuring orientation with MEMS accelerometers in a centrifuge. *IFCEE*. ASCE, San Antonio.

Bennett, V., Abdoun, T., Shantz, T., Jang, D. & Thevanayagam, S., 2009. Design and characterization of a compact array of MEMS accelerometers for geotechnical instrumentation. Smart Struct. and Syst. Techno-Press **5**(**6**): 663–679

Bhattacharya, S., Murali Krishna, A., Lombardi, D., Crewe, A. & Alexander, N., 2012. Economic MEMS based 3-axis water proof accelerometer for dynamic geo-engineering applications. Soil

Dyn. Earthquake Eng. Elsevier **36** 111–118

Black, J.A., Baker, N. & Ainsworth, A., 2014. Establishing a 50 g-ton geotechnical centrifuge at the University of Sheffield. *8th Int. Conf. on Phys. Model. in Geotech.* Perth, Australia, pp. 181–186.

Blake, A.P. & O'Loughlin, C.D., 2015. Installation of dynamically embedded plate anchors as assessed through field tests. Can. Geotech. J. NRC Research Press **52**(**9**): 1–13

Chow, S.H., O'Loughlin, C.D., Corti, R., Gaudin, C. & Diambra, A., 2015. Drained cyclic capacity of plate anchors in dense sand : Experimental and theoretical observations. Geotechnique Letters. ICE **5**(**2**): 80–85

DNV, 2007. *Offshore standard DNV-OS-J101: design of offshore wind turbine structures*. Hovik, Norway.

Elgamal, A., Dobry, R. & Van Laak, P., 1991. Design, construction and operation of 100 g-ton centrifuge at RPI. *Centrifuge 91*. Boulder, CO, pp. 27–34.

Ellis, E., Cox, C., Yu, H., Ainsworth, A. & Baker, N., 2006. A new geotechnical centrifuge at the University of Nottingham, UK. *6th Int. Conf. Phys. Model. Geotech.* CRC Press, Hong Kong, pp. 129–133.

Hoffman, K., Varuso, R. & Fratta, D., 2006. The use of low-cost MEMS accelerometers for the near-surface monitoring of geotechnical engineering systems. *GeoCongress 2006*. ASCE, Atlanta, pp. 1–6.

Lau, B.H., 2015. *Cyclic behaviour of monopile foundations for offshore wind farms*. University of Cambridge, Cambridgeshire.

Leung, a. M., Jones, J., Czyzewska, E., Chen, J. & Pascal, M., 1997. Micromachined accelerometer with no proof mass. International Electron Devices Meeting. IEDM Technical Digest. 899–902

Madabhushi, G., 2015. *Centrifuge modeling for civil engineering*. CRC Press, Boca Rotan, FL.

522 MEMSIC, *CXL-GP series general purpose accelerometer*. San Jose, CA.

523 MEMSIC, 2007. *Ultra Low Noise , Offset Drift ± 1 g Dual Axis Accelerometer with Analog*
524 *Outputs*. Andover, MA.

525 O'Loughlin, C.D., Gaudin, C., Morton, J.P. & White, D.J., 2014. MEMS accelerometers for
526 measuring dynamic penetration events in geotechnical centrifuge tests. Int. J. of Phys. Modell.
527 in Geotech. ICE **14**(**2**): 1–9

528 Oppenheim, I.J., Garrett Jr., J.H. & Ganerial, K.J., 2000. Potential MEMS applications in civil
529 engineering. *Space 2000*. ASCE, Albuquerque, pp. 495–501.

530 Randolph, M.F., Jewell, R.J., Stone, K.J.L. & Brown, T.A., 1991. Establishing a new centrifuge
531 facility. *Centrifuge 91*. Balkema, Boulder, CO.

532 Saftner, D.A., Green, Russell, A., Hryciw, R.D. & Lynch, J.P., 2008. Instrumentation for the
533 NEESR sand aging field experiment. *GeoCongress 2008*. ASCE, New Orleans.

534 Schofield, A.N., 1969. Cambridge geotechnical centrifuge operations. Géotechnique. ICE **30**(**3**):
535 227–268

536 Shaeffer, D.K., 2013. MEMS inertial sensors: A tutorial overview. IEEE Communications
537 Magazine. IEEE **51**(**April**): 100–109

538 Silicon Design Inc., 2013. *Model 2012*. Kirkland, WA.

539 Spangler, L. "Chip" & Kemp, C.J., 1996. ISAAC: integrated silicon automotive accelerometer.
540 Sensors and Actuators A: Physical. Elsevier **54**(**1**–**3**): 523–529

541 Stark, N., Kopf, A., Hanff, H., Stegmann, S. & Wilkens, R., 2009. Geotechnical investigations of
542 sandy seafloors using dynamic penetrometers. OCEANS 2009, MTS/IEEE Biloxi - Marine
543 Technology for Our Future: Global and Local Challenges.

544 Stratasya, 2015. Fortus: 380mc and 450 mc. Stratasy,.

545 Stringer, M., Heron, C. & Madabhushi, S., 2010. Experience using MEMS-based accelerometers in
546 dynamic testing. *Proc. of the 7th Int. Conf. on Phys. Model. in Geotech.* (C. Gaudin & D.
547 White (eds.)). CRC Press, Perth, pp. 389–394.

548 Taboada-Urtuzuástegui, V.M. & Dobry, R., 1998. Centrifuge modeling of earthquake-induced
549 lateral spreading in sand. J. Geotech. Geoenviron. Eng. ASCE **124**(**12**): 1195–1206

550 Wong, H.L. & Trifunac, M.D., 1977. Effects of cross-axis sensitivity and misalignment on the
551 response of mechanical-optical accelerographs. Bull. Seismol. Soc. Am. Seismological Society
552 of America **67**(**3**): 929–956.

553

554

Figure captions

Figure 1. Example of using MEMS accelerometer to measure cyclic moment loading of a caisson. Load eccentricity is 3.05 caisson diameter

Figure 2. Centrifuge gravity and model coordinate system from Beemer et al. (2017)

Figure 3. 3D printed 1-g MEMS accelerometer calibrator

Figure 4. Applied and measured accelerations by a MEMS Accelerometer (not to scale)

Figure 5. Apparent internal misalignment of the MEMS accelerometer in the x-z plane

Figure 6. Sketch of experiment within the centrifuge (not to scale), α and β are assumed to be negligible

Figure 7. Experiment sketch with geometry and gravity (not to scale), β is assumed to be negligible

Figure 8. Sensors at Zero Degree Angle in Experiment Three Data

Figure 9. Measured Cross-Axis Acceleration versus Centrifuge Gravity with curve fitting, M1, M2, and M7

Figure 10. Results from cross-axis correction validation experiment a) Platform One b) Platform Two c) Platform Three

Table captions

Table 1. Accelerometer Technical Specifications

Table 2: 10 g Accelerometer Calibration Properties

Table 3. Experiment Targeted and Applied Reactive Centrifugal Acceleration

Table 4. Sensor Configuration per Experiment

Table 5. Measured Differential Rotation of Centrifuge Basket

Table 6: Results from High-g Cross-Axis Calibration of 10g Accelerometers

Table 7. Cross-Axis Sensitivity Validation

Figure01

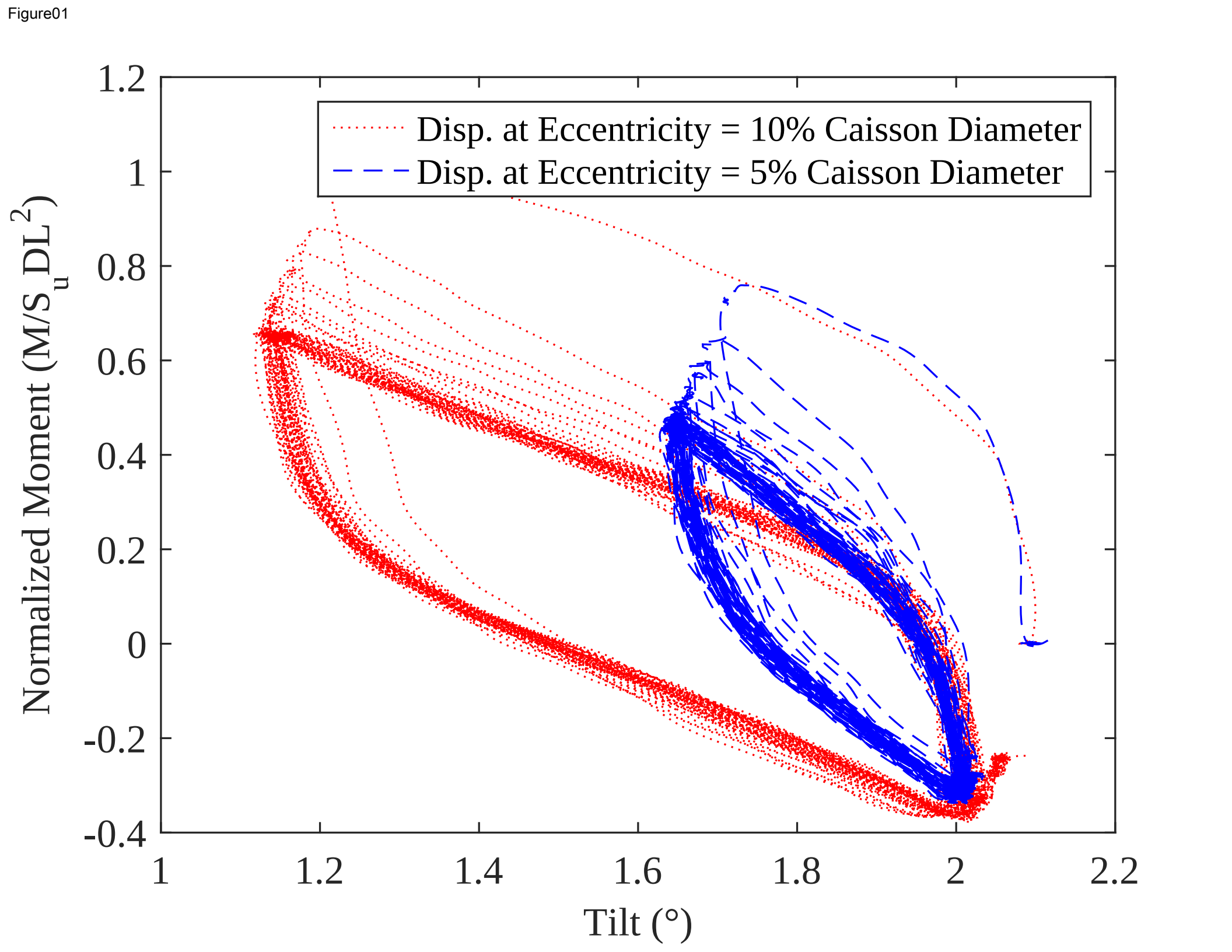
Disp. at Eccentricity = 10% Caisson Diameter
Disp. at Eccentricity = 5% Caisson Diameter
Normalized Moment (M/S$_u$DL^2)
Tilt (°)
1.2
1
0.8
0.6
0.4
0.2
0
-0.2
-0.4
1
1.2
1.4
1.6
1.8
2
2.2

Figure02

Centrifuge Axis, Y
Centrifuge Radius, r
R
Model
x
z
ρ_2
β
α
$\xi=\alpha+\beta$

Figure03

Click here to download Figure Beemerfig03.JPG

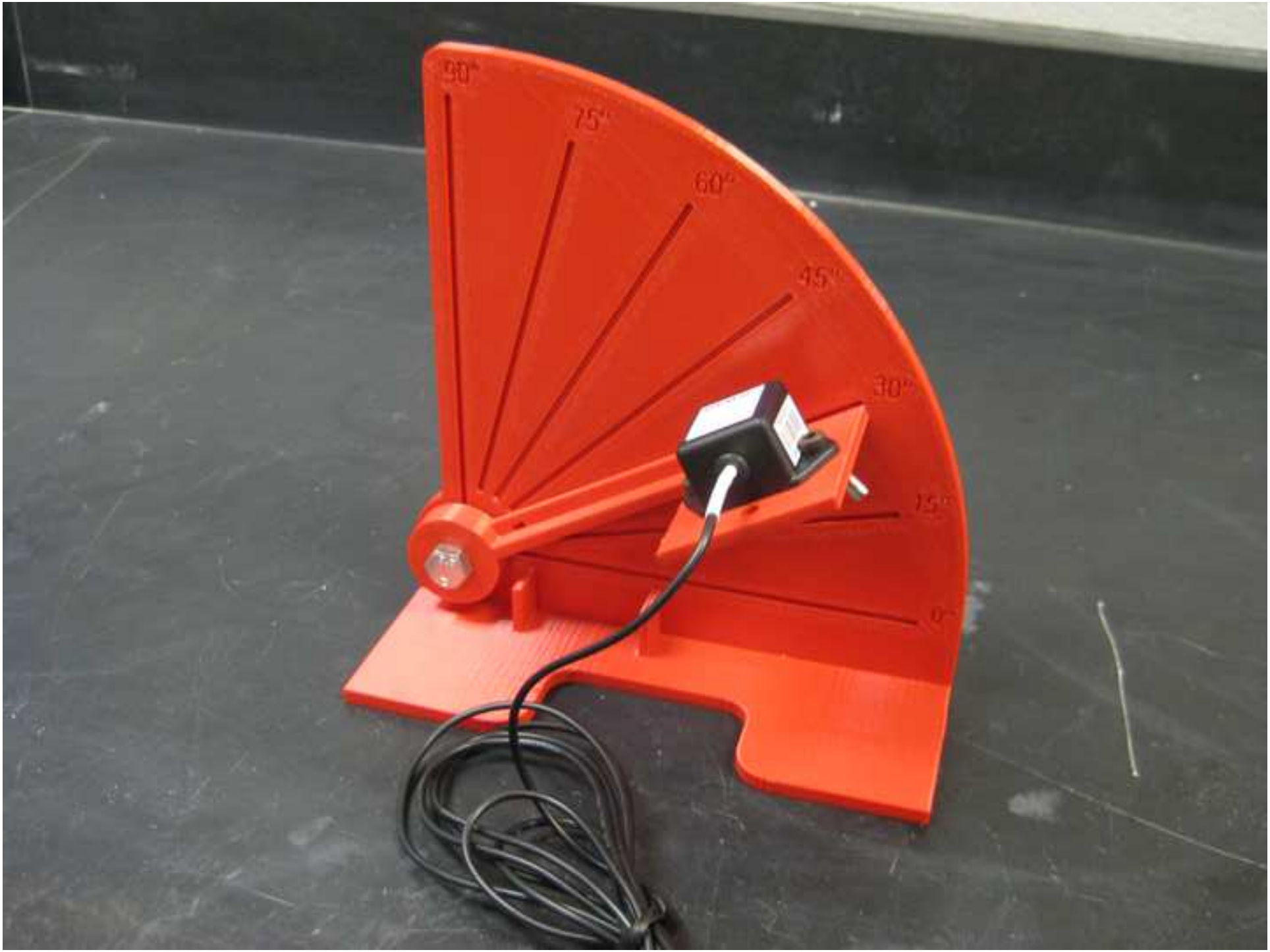

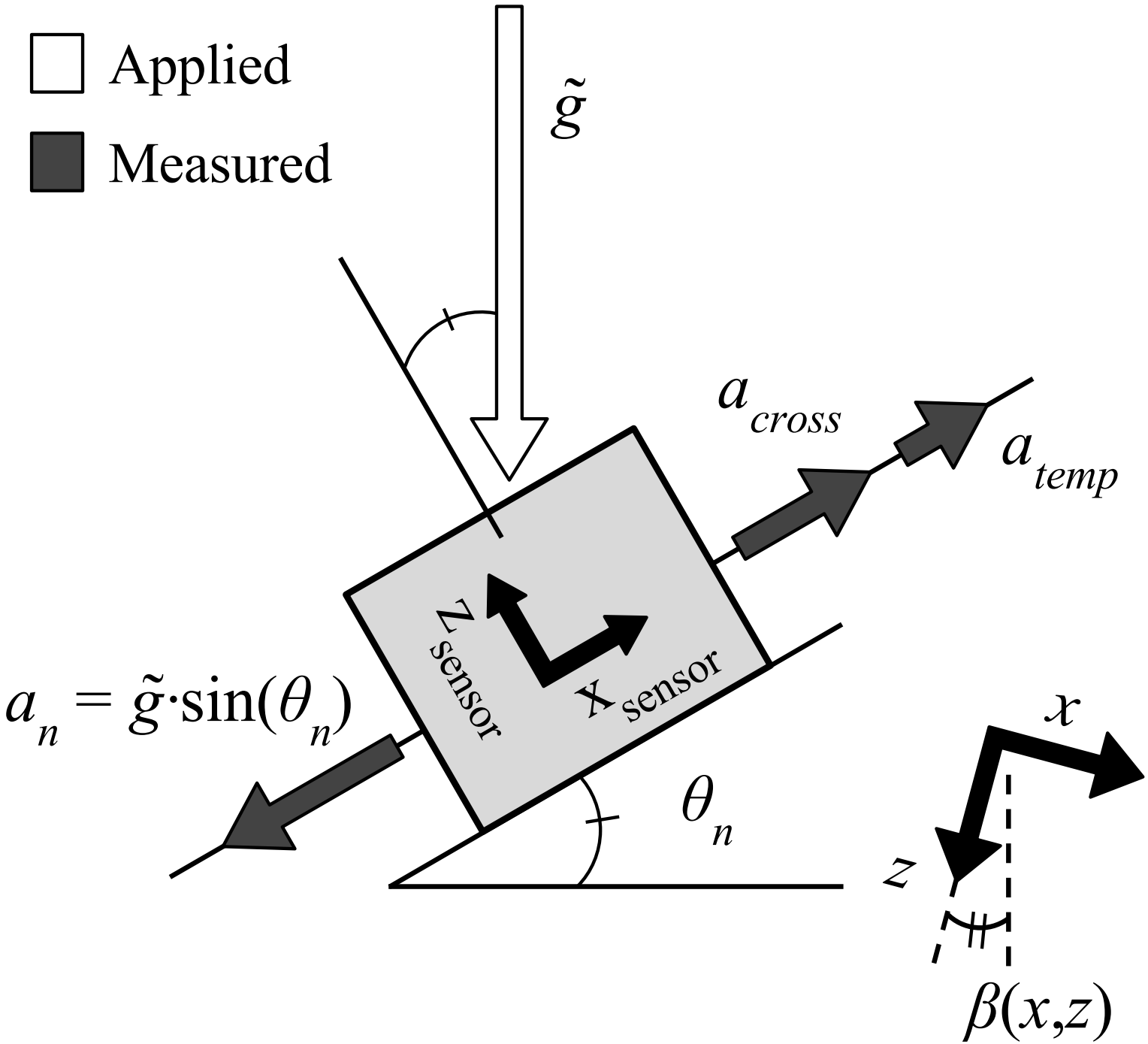

Measurement Axis: x_{sensor}

Figure04

Figure05

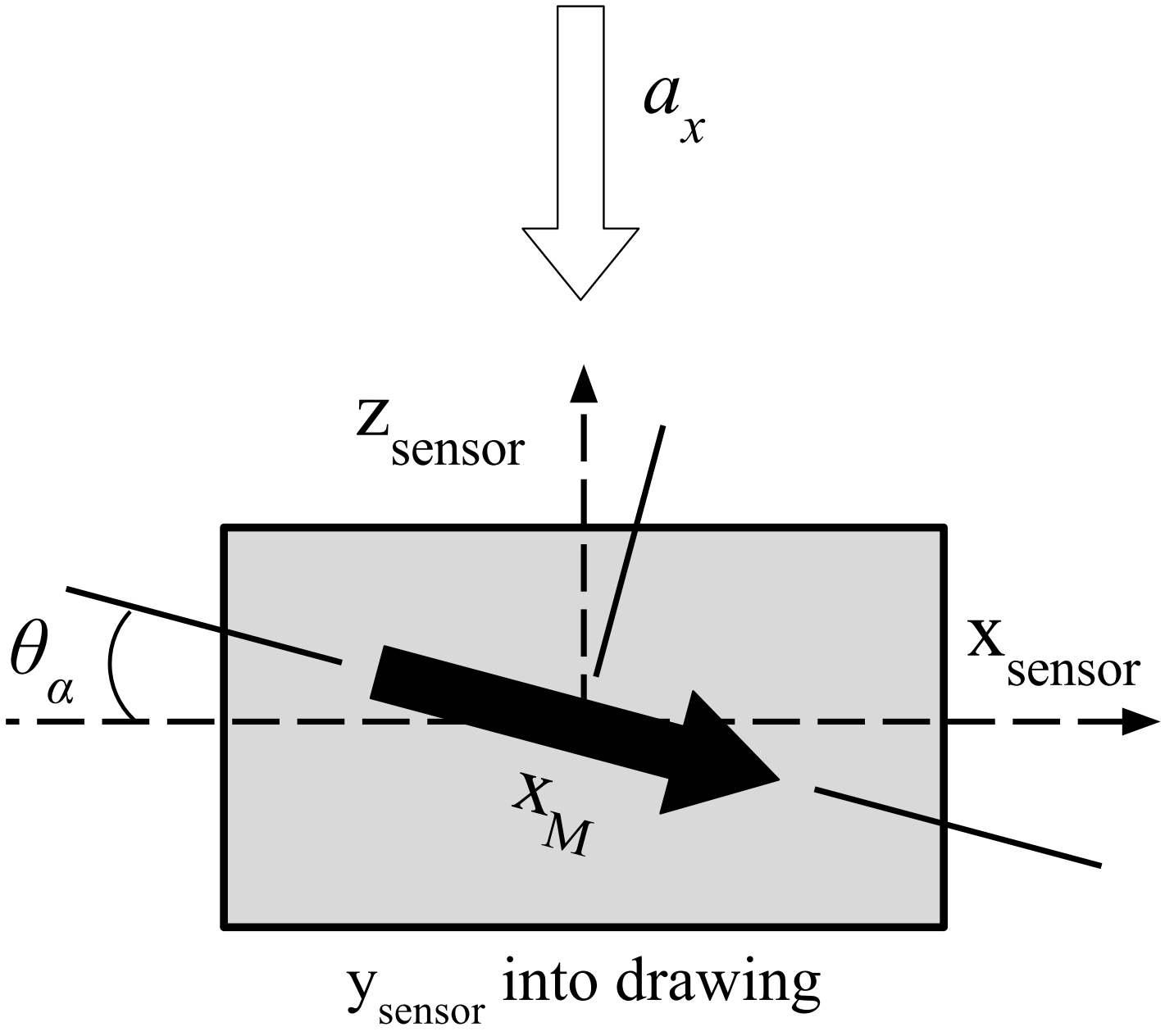

Defined Measurement Axis: x_{sensor}
Apparent Measurement Axis: x_M

Figure06

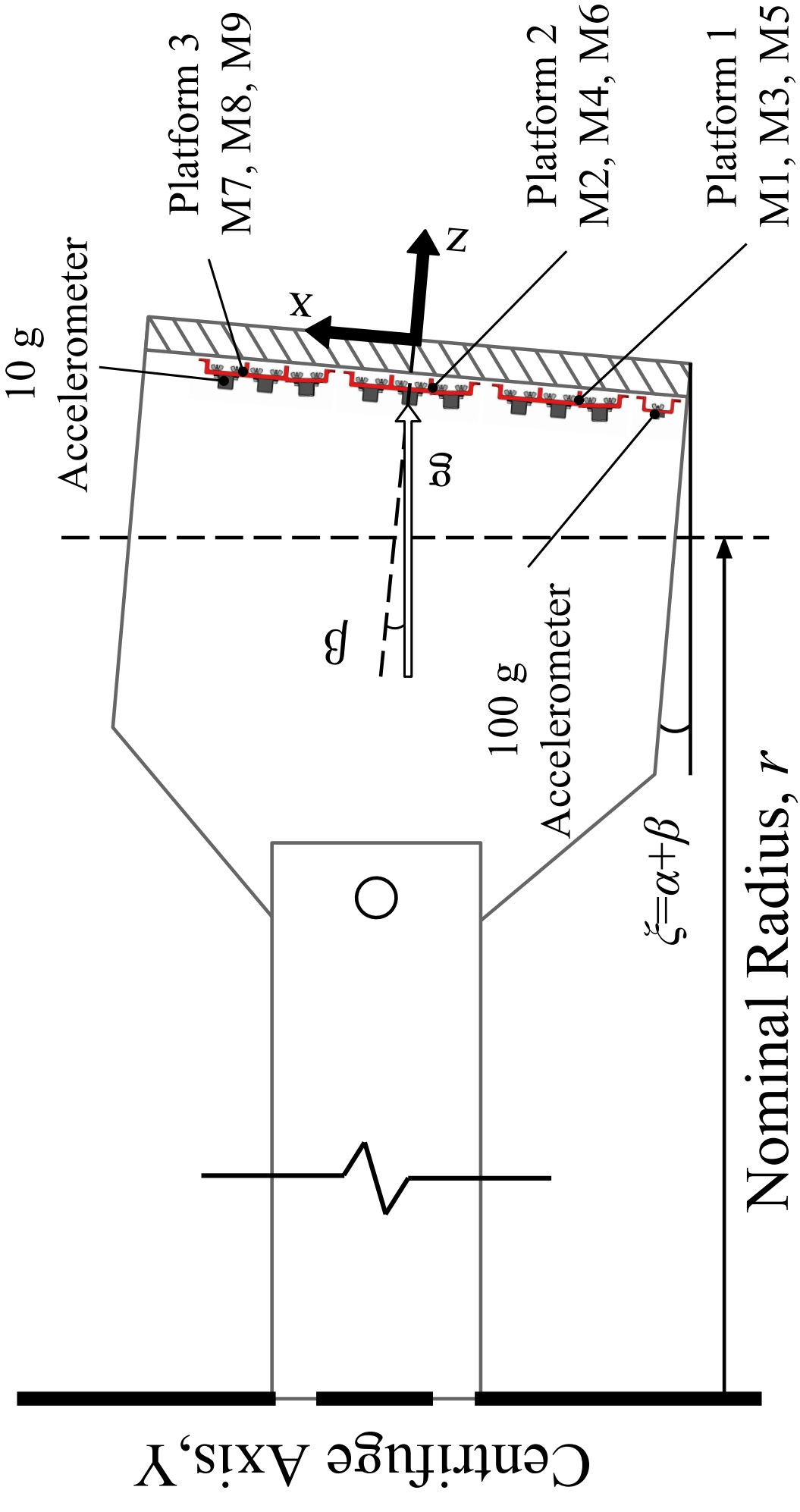
Platform 3
M7, M8, M9
Platform 2
M2, M4, M6
Platform 1
M1, M3, M5
10 g
Accelerometer
z
x
ω
β
100 g
Accelerometer
ζ=α+β
Nominal Radius, r
Centrifuge Axis, Y

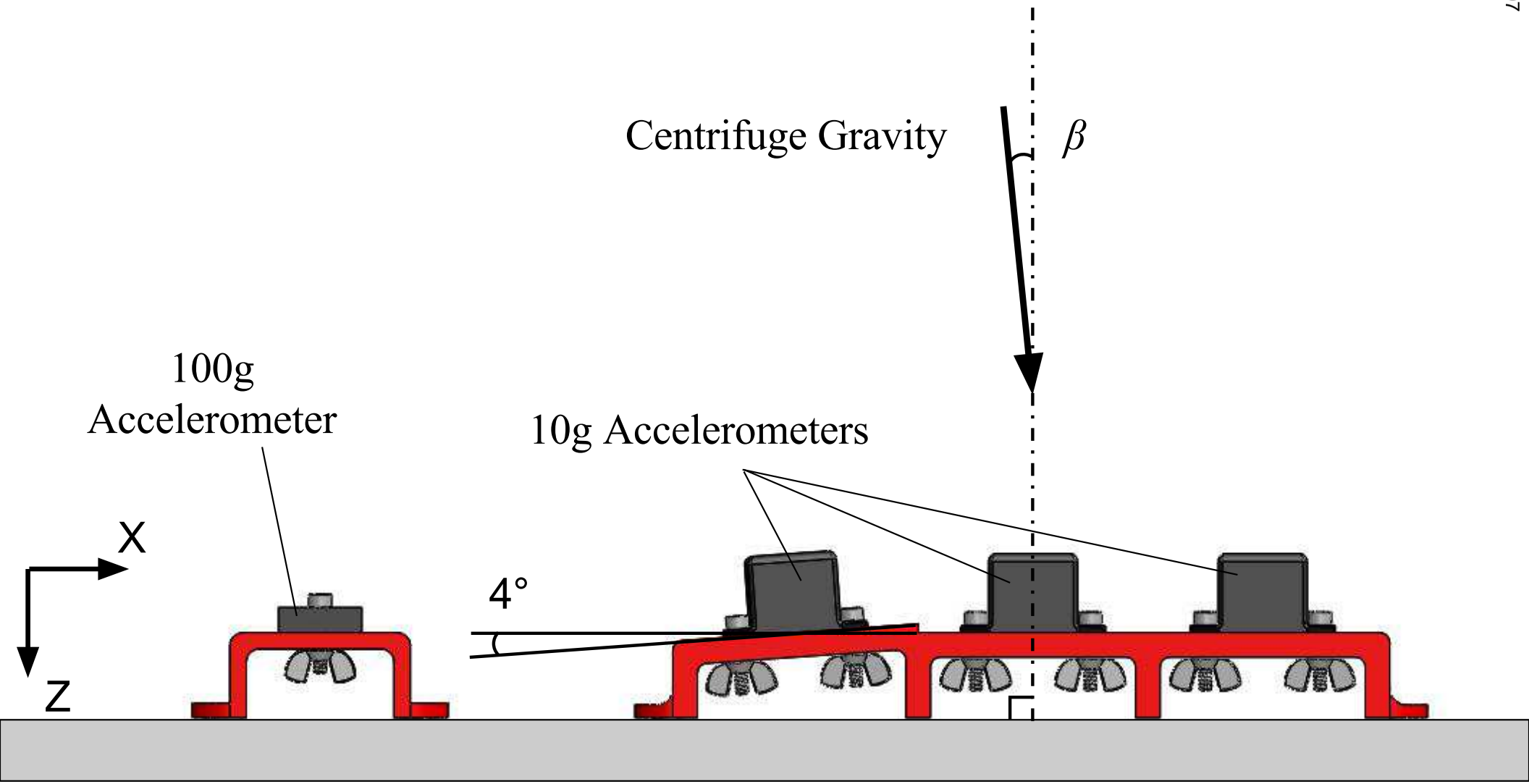
Centrifuge Gravity
β
100g
Accelerometer
10g Accelerometers
X
Z
4°

Figure07

Figure08

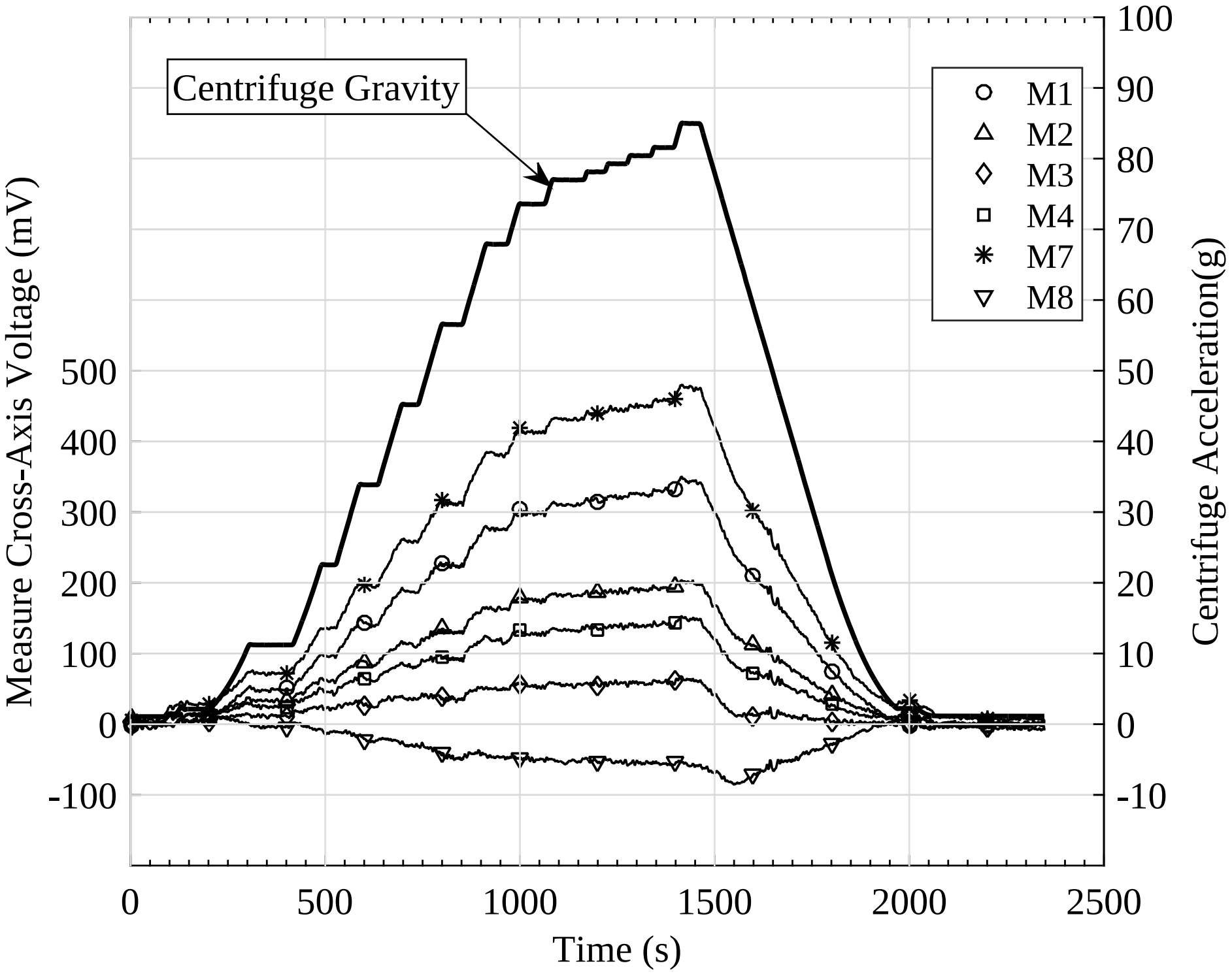
Centrifuge Gravity
M1
M2
M3
M4
M7
M8
Measure Cross-Axis Voltage (mV)
Centrifuge Acceleration(g)
Time (s)
500
400
300
200
100
0
-100
100
90
80
70
60
50
40
30
20
10
0
-10
0
500
1000
1500
2000
2500

Figure09

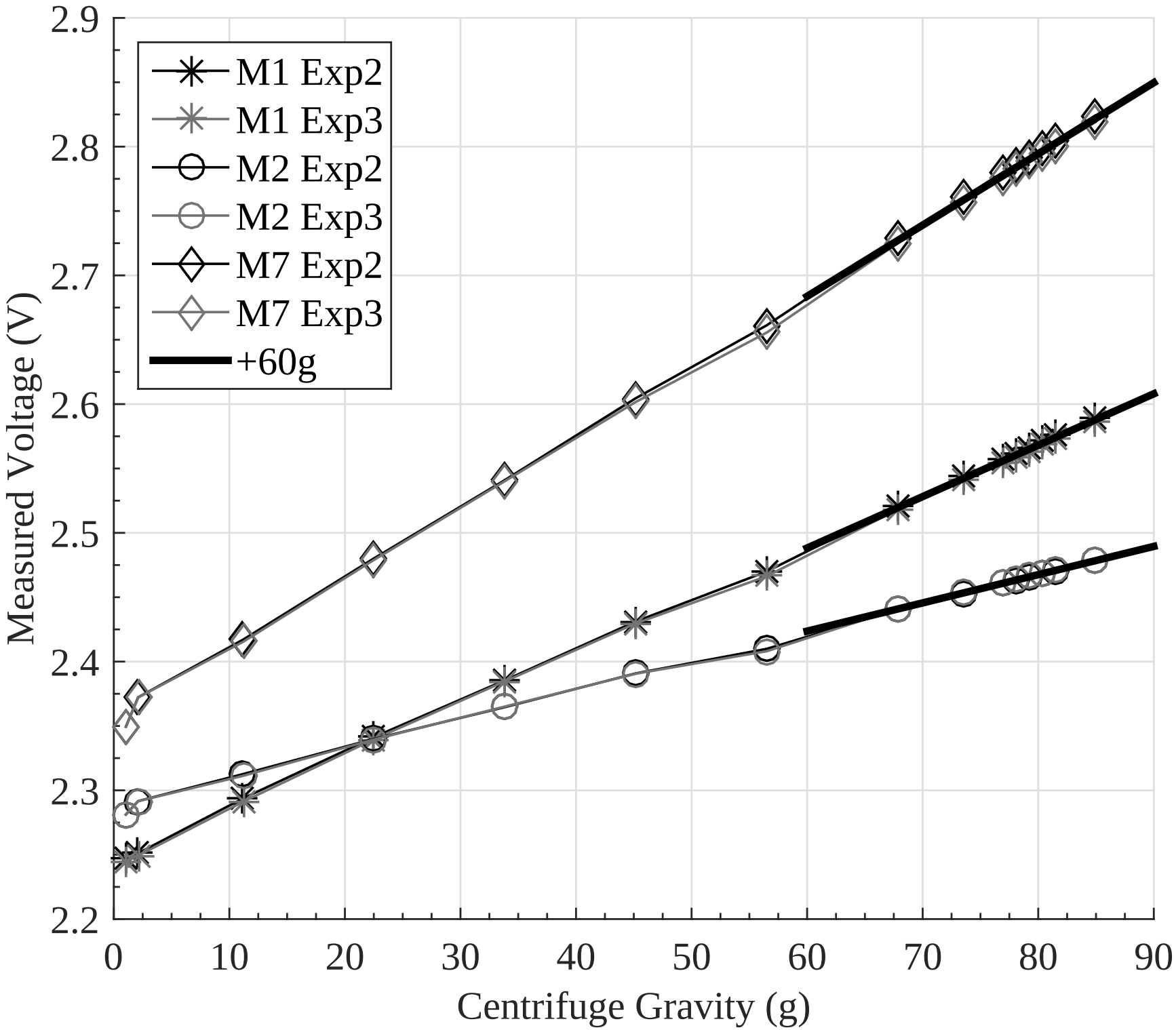
M1 Exp2
M1 Exp3
M2 Exp2
M2 Exp3
M7 Exp2
M7 Exp3
+60g
Measured Voltage (V)
Centrifuge Gravity (g)
2.2
2.3
2.4
2.5
2.6
2.7
2.8
2.9
0
10
20
30
40
50
60
70
80
90

Figure10

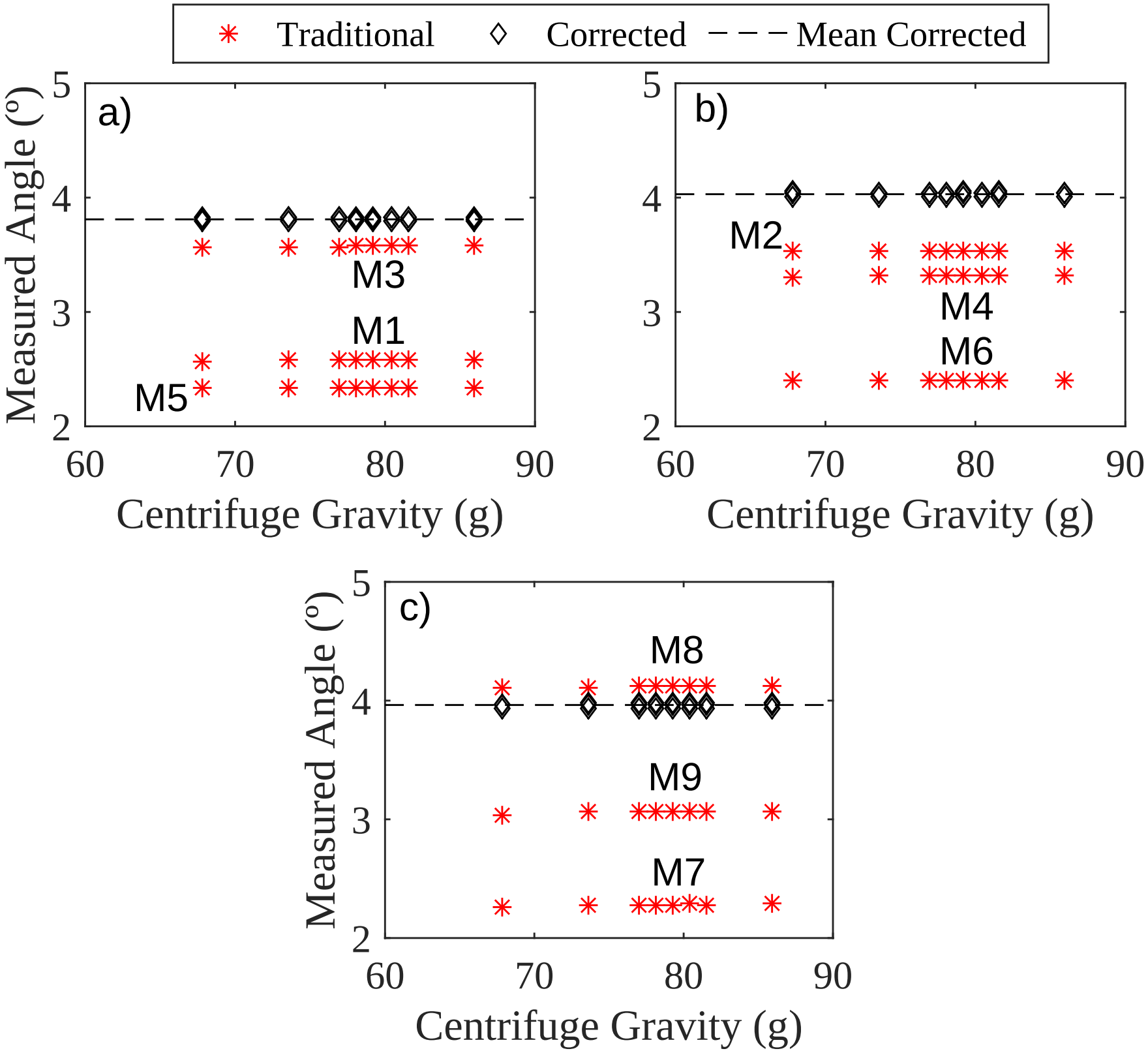
Traditional
Corrected
Mean Corrected
a)
b)
c)
M1
M2
M3
M4
M5
M6
M7
M8
M9
Measured Angle (°)
Centrifuge Gravity (g)
2
3
4
5
60
70
80
90

Table 1: Accelerometer Technical Specifications

	10 g Accelerometer	100 g Accelerometer
Sensitivity (mV/g)	200 ± 5	40
Zero-g Voltage (V)	2.375 ± 0.1	2.50 (Single Ended)
Span Output (V)	±2.0 ± 0.1	±2.0 (Single Ended)
Cross-Axis Sensitivity	± 5 (% of Span)	2 (%) TYP
Alignment Error (°)	±2	-
Noise (mg rms)	35	0.140
Temperature Offset	± 0.3 g (0º-70º C)	$5x10^{-3}$ g/ºC

Table 2: 10 g Accelerometer Calibration Properties

Sensor	$C_{F\alpha}$ (g/V)	V_{α} (V)
M1	4.982	2.243
M2	5.044	2.279
M3	5.068	2.321
M4	5.086	2.366
M5	4.993	2.214
M6	4.997	2.252
M7	4.949	2.344
M8	5.087	2.238
M9	5.029	2.240

Table 3: Applied Cross-Axis Centrifuge Gravity

Step	Experiment One	Experiments Two and Three
	Centrifuge Gravity (g)	
1	1.00	1.05
2	2.06	2.12
3	22.44	11.19
4	45.09	22.51
5	67.77	33.84
6	73.46	45.17
7	76.87	56.51
8	78.01	67.86
9	79.16	73.55
10	80.29	76.97
11	81.44	78.10
12	84.86	79.25
13	-	80.40
14	-	81.54
15	-	85.95

Table 4: Sensor Configuration per Experiment

Platform	Sensor	Experiment One	Experiment Two	Experiment Three
		Orientation (°)		
1	M1	4	0	0
	M3	0	4	0
	M5	0	0	4
2	M2	4	0	0
	M4	0	4	0
	M6	0	0	4
3	M7	4	0	0
	M8	0	4	0
	M9	0	0	4

Table 5: Measured Differential Rotation of Centrifuge Basket

ΔExp	Sensor	Exp One	Exp Two	Exp Three	$\Delta\theta_\alpha$ (°)
		Misalignment, θ_α, (°)			
1-2	M3	0.43	-	0.21	0.23
	M4	0.67	-	0.50	0.17
	M8	0.075	-	-0.18	0.25
				Mean:	0.22
1-3	M5	1.64	1.41	-	0.24
	M6	1.79	1.56	-	0.23
	M9	1.08	0.86	-	0.22
				Mean:	0.22
2-3	M1	-	1.17	1.16	0.02
	M2	-	0.64	0.64	0.00
	M7	-	1.62	1.60	0.02
				Mean:	0.01

Table 6: Results from High-g Cross-Axis Calibration of 10g Accelerometers

Sensor	C_x	R^2	θ_α	C_F	V_0
	(mV/g)	-	(°)	(g/V)	(V)
M1	3.99	0.999	1.16	5.086	2.247
M2	2.19	0.999	0.64	5.101	2.281
M3	0.72	0.991	0.21	5.086	2.321
M4	1.62	0.999	0.48	5.129	2.367
M5	4.81	0.999	1.41	5.119	2.219
M6	5.30	0.999	1.56	5.137	2.257
M7	5.56	0.999	1.61	5.093	2.349
M8	-0.56	0.973	-0.16	5.073	2.237
M9	2.93	0.999	0.86	5.105	2.243

Table 7: Cross-Axis Sensitivity Validation

Platform	Experiment	Sensor	Average Measured Angle (°) Note: Platform Angle is 4°	
			Cross-Axis Correction	
			✖	✓
One	1	M1	2.58	3.81
	2	M3	3.58	3.80
	3	M5	2.33	3.82
Two	1	M2	3.32	4.01
	2	M4	3.53	4.04
	3	M6	2.40	4.04
Three	1	M7	2.28	3.98
	2	M8	4.12	3.94
	3	M9	3.06	3.97